CrossMark

Improvement of Microstructure and Mechanical Properties of CoCrCuFeNi High-Entropy Alloys By V Addition

Gang Qin, Shu Wang, Ruirun Chen, Huiting Zheng, Liang Wang, Yanqing Su, Jingjie Guo, and Hengzhi Fu

V element had positive effect in improving the strength of many alloys, so it was possible that V had potential to strengthen CoCrCuFeNi high-entropy alloys (HEAs) with face-centered cubic (FCC) crystal structure, which was relatively weak in strength and had outstanding ductility. In this paper, we studied the alloying effect of V on the phase evolution, microstructure and the mechanical properties of the $(CoCrCuFeNi)_{100-x}V_x$ ($x = 0$-16, atomic ratio, hereafter in at.%) HEAs systematically. The results showed that V element had capacity to induce sigma phase precipitation. The volume fraction of sigma phase increased from 0 to 12%; the compressive yield stress of $(CoCrCuFeNi)_{100-x}V_x$ HEAs increased from 300 to 613 MPa with V content increasing from 0 to 16% (atomic ratio, hereafter in at.%). However, the compression fracture strain decreased from 50 to 28%. V addition was beneficial in improving the strength of CoCrCuFeNi HEA, and the increase in sigma phase volume fraction was the key factor for the improvement of the $(CoCrCuFeNi)_{100-x}V_x$ HEAs in yield stress.

1. Introduction

High-entropy alloys (HEAs) were firstly proposed by Yeh and Cantor in 2004 (Ref 1, 2). They had been a new hot topic in metal material field because of their excellent mechanical properties (Ref 3-23). It was an important breakthrough in the traditional metallic materials field; it also opened a new path to study and develop new metal material with outstanding mechanical properties.

For traditional alloy materials, one or two elements were selected as the major component based on the primary property requirement, and other alloy elements were added in the matrix for conferring the secondary properties without altering the primary properties of the matrix (Ref 2). Some similar methods were also used in HEAs field, and some studies had revealed that the addition of alloying elements had positive effect on the microstructure and mechanical properties. For example, Stepanov et al. (Ref 24) had studied the effect of V element on microstructure and mechanical properties of the CoCrFeMnNiV_x HEAs and they found that the sigma phase was generated in the matrix, the volume fraction of sigma phase

increased with increasing V content, and the strength increased with increasing volume fraction of sigma phase. Wang et al. (Ref 25) investigated the microstructure and mechanical properties of CoCrCuFeNiTi_x HEAs. They found that the compression strength increased and the magnetic conversion changed from paramagnetism to superparamagnetism as Ti content increased. The correlation between the microstructure and mechanical properties of the $(FeCoNiCrMn)_{100-x}Al_x$ HEAs also was presented by He et al. (Ref 26). They found that the phase structure transformed from the FCC to BCC structure and the mechanical properties increased in strength but reduced in ductility with increasing Al content (Ref 26). Li et al. concluded the effect of the Mn, Ti and V addition on microstructure and mechanical properties of AlCrFeCoNiCu HEA, and they found that these three elements had positive effect on phase evolution and performance optimization. The V element showed the best strengthening effect and the lowest decreases in the ultimate strain on AlCrFeCoNiCu HEA (Ref 27). The effect of V element on microstructure and mechanical properties of AlCoCrFeNiV_x was reported by Dong et al. (Ref 28). They found that the Vickers hardness increased with an increase in the V content and the fine nanoscale spinodal decomposition microstructure had a major contribution to the high fracture strength of the AlCoCrFeNiV_{0.2} HEA. Wang et al. reported the effect of Al addition on the microstructure and mechanical properties of Al_xCoCrFeNi HEAs. The research showed that the hardness was increased by generating BCC phase, and the volume fraction of BCC phase increased as the Al content increased (Ref 29). Table 1 summarizes the alloy effect of some reported alloy elements on the phase structure and mechanical properties of some HEAs. These reports (Ref 24-38) focus on the effect of some alloy elements on phase precipitation, microstructure and mechanical properties of some HEAs. They indicated that some elements had positive effect in improving the strength of HEAs. CoCrCuFeNi high-entropy alloys (HEAs) possessed face-centered cubic (FCC) crystal structure, which was relatively weak in strength and had

Gang Qin, Shu Wang, Huiting Zheng, Liang Wang, Yanqing Su, Jingjie Guo, and **Hengzhi Fu**, National Key Laboratory for Precision Hot Processing of Metals, Harbin Institute of Technology, Harbin 150001, China; **Ruirun Chen**, National Key Laboratory for Precision Hot Processing of Metals, Harbin Institute of Technology, Harbin 150001, China; and State Key Laboratory of Advanced Welding and Joining, Harbin Institute of Technology, Harbin 150001, China. Contact e-mail: ruirunchen@hit.edu.cn.
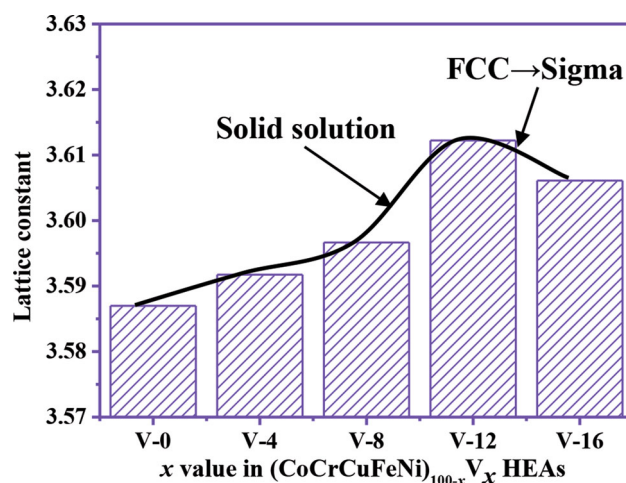
Table 1   Effect of some reported alloy elements on the phase structure and mechanical properties of some HEAs

Basis material	Alloy element	Second phase	Yield strength	Fracture strain
CoCrFeMnNi (Ref 24)	V	Sigma	Up	Down
CoCrCuFeNi (Ref 25)	Ti	Laves	Up	Down
CoCrFeMnNi (Ref 26)	Al	BCC	Up	Down
AlCoCrFeNi (Ref 28)	V	Nanoscale decomposition	Up	Down
CoCrFeNi (Ref 29)	Al	BCC	Up	Down
CoCrFeNi (Ref 30)	Mo	δ	Up	Down
CoCrFeNi (Ref 31, 34)	Nb	Laves	Up	Down
AlCoCrFeNi (Ref 32)	Nb	Laves	Up	Down
AlCoCrFeNi (35)	Zr	Leave	Up	Down
AlCoCrFeNi (Ref 38)	Si	δ	Up	Down
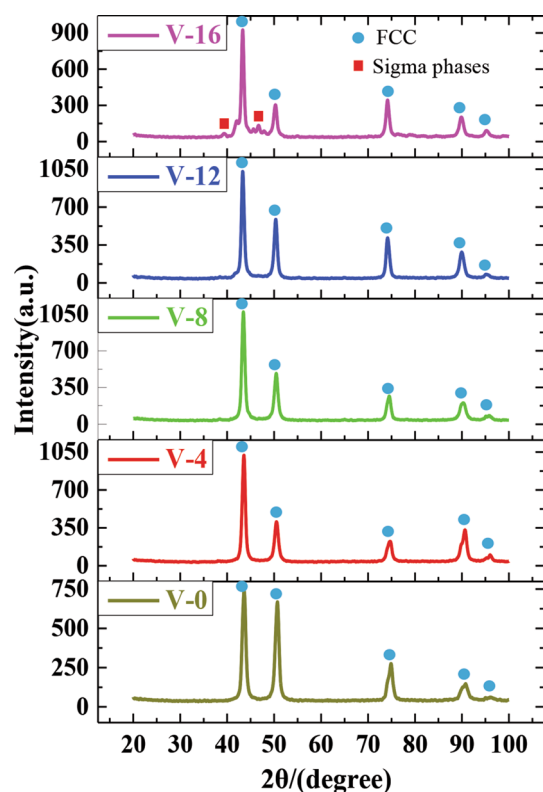
Fig. 1   XRD patterns of $(CoCrCuFeNi)_{100-x}V_x$ (x = 0, 4, 8, 12 and 16) HEAs

Fig. 2   Lattice constant of $(CoCrCuFeNi)_{100-x}V_x$ (x = 0, 4, 8, 12 and 16) HEAs attained by XRD

outstanding ductility (Ref 25). V element had positive effect in improving the strength of some HEAs (Ref 24, 28), so it was possible that V had potential in strengthening this CoCrCuFeNi HEA. However, the effect of V addition on the microstructure and mechanical properties of CoCrCuFeNi HEA had not been reported based on the previous reports (Ref 5, 24-39) and this gap should be filled.

In this paper, the CoCrCuFeNi HEA (all elements in equal atomic proportions) with a single FCC phase solid solution was selected as matrix. The alloying effect of V element on the phase evolution, microstructure and mechanical properties of the $(CoCrCuFeNi)_{100-x}V_x$ (x = 0-16, atomic ratio, hereafter in at.%) HEAs was studied systematically. Furthermore, the relationship between the microstructure and mechanical properties was investigated and the strengthening mechanism of V element on CoCrCuFeNi HEA was also revealed.

2. Experimental

The ingots of $(CoCrCuFeNi)_{100-x}V_x$ (x = 0-16 at.%) HEAs were prepared by arc melting in a copper mold under high-purity argon atmosphere. The metal powders (Co, Cr, Cu, Fe, Ni and V) with purity more than 99% were selected to be the raw material. For the chemical composition uniformity, each ingot was smelted seven times. We used electric discharging machining to cut the ingots into several shapes for detecting. The x-ray diffraction (XRD) using Cu K_α radiation (MXP21VAHF) scanning from 20° to 100° in 2θ at a scanning rate of 4°/min identified the phase structures of the HEAs. The specimens were observed by scanning electron microscopy (SEM) using a Zeiss Supra 55 instrument operated at 15 kV and equipped with an energy-dispersive spectrometer (EDS) to analyze the chemical composition distribution. The SEM samples were grounded, polished and electro-polished in the corrosive liquid of 90% acetic acid and 10% perchloric acid mixture at room temperature and an applied voltage of 27 V for 15 s. The diameter and the height of the compression samples were, respectively, 4 and 6 mm. Compression tests were carried out on an AG–X Plus 250-kN electronic universal material testing machine at a strain rate of 0.5×10^{-3} m/min at room temperature; for each specimen, at least 3 samples were measured to acquire an accurate value.
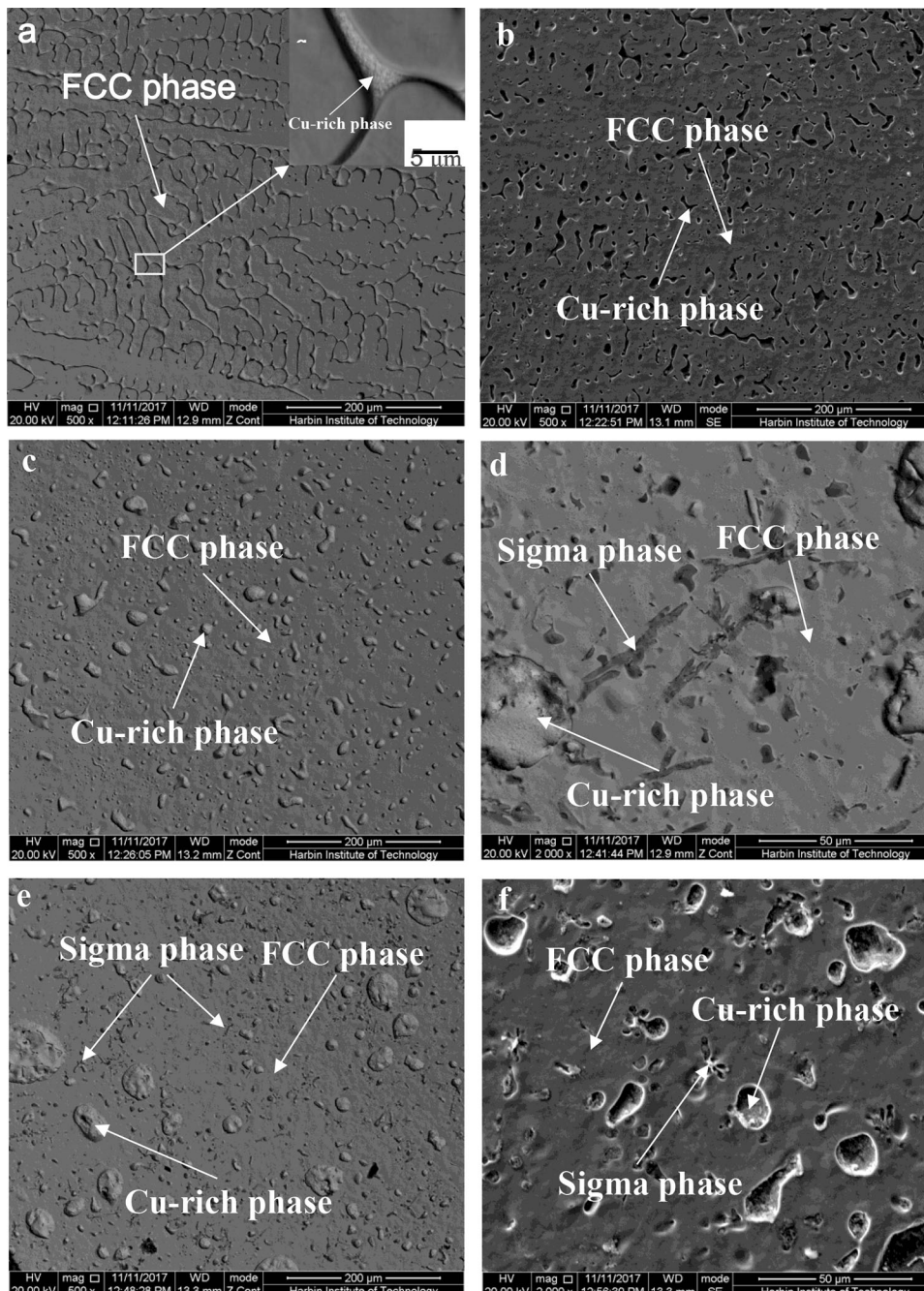
Fig. 3 SEM images of the as-cast $(CoCrCuFeNi)_{100-x}V_x$ alloys. (a–e represent the SEM images of CoCrCuFeNi $(CoCrCuFeNi)_{96}V_4$, $(CoCrCuFeNi)_{92}V_8$, $(CoCrCuFeNi)_{88}V_{12}$, $(CoCrCuFeNi)_{84}V_{16}$ HEAs, and (f) represents the image of $(CoCrCuFeNi)_{84}V_{16}$ HEA with high magnification), (g) represents the high-magnification image of the interdendritic region in CoCrCuFeNi HEA

3. Results and Discussion

The XRD patterns showed that the sigma phase precipitated in the $(CoCrCuFeNi)_{100-x}V_x$ HEAs with increasing V content. The duplex-phase structure had better solid-solution strengthening effect than single-phase structure (Ref 40). As shown in Fig. 1, only patterns related FCC phase structure was detected when V content was 0-12%. The sigma phase precipitated until V content reached 16%. It implied that V addition had positive effect on phase precipitation from FCC phase to sigma phase in the $(CoCrCuFeNi)_{100-x}V_x$ HEAs. As shown in Fig. 2, the

lattice constant showed a rising tendency when V content increased from 0 to 12%, while the lattice constant decreased when V content increased from 12 to 16%. The main factor was that some atoms were dissolved in this matrix when V content increased from 0 to 12%, which contributed to the increases in lattice constant. When V content reached 12%, the sigma phase was precipitated, which released the lattice distortion energy, so the lattice constant was decreased (Ref 16-18, 36).

To analyze the microstructure, the polished samples were observed by SEM and the elements distribution maps were also attained by EDS. Figure 3 shows the microstructures of the $(CoCrCuFeNi)_{100-x}V_x$ HEAs. When V content was 0%, as
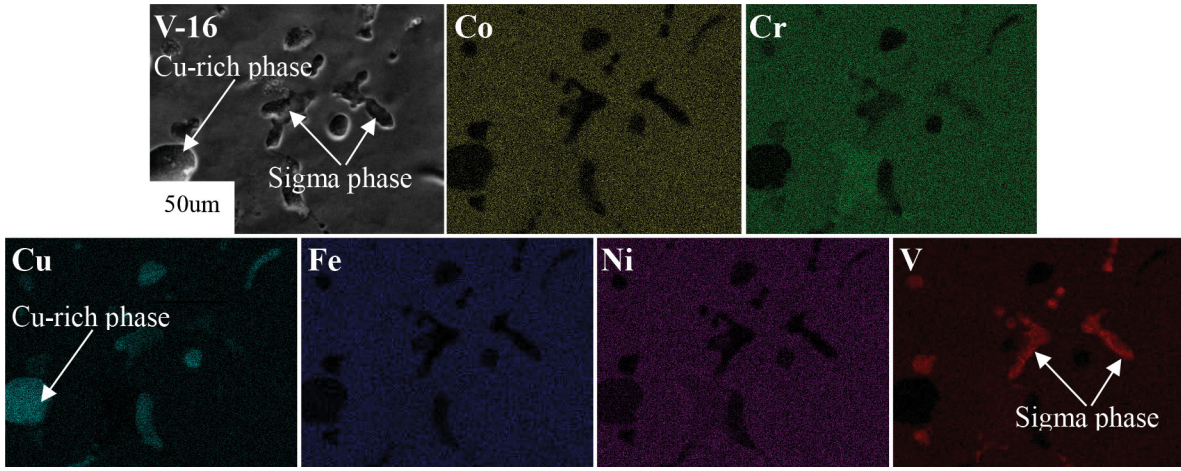
Fig. 4 Elements distribution of $(CoCrCuFeNi)_{84}V_{16}$ HEA by EDS analysis

Table 2 Compositions (at.%) of various phases in the as-cast $(CoCrCuFeNi)_{100-x}V_x$ (x = 0, 4, 8, 12 and 16) HEAs

HEA	Region	Co	Cr	Cu	Fe	Ni	V
CoCrCuFeNi	Nominal	20	20	20	20	20	0
	Dendritic	21.86	22.72	10.62	18.71	26.08	0
	Interdendritic	4.45	3.67	76.85	3.91	11.12	0
$(CoCrCuFeNi)_{96}V_4$	Nominal	19.2	19.2	19.2	19.2	23	4
	FCC phase	23.31	22.19	9.09	21.02	19.71	4.46
	Cu-rich phase	3.52	3.22	81.12	3.25	8.89	0
$(CoCrCuFeNi)_{92}V_8$	Nominal	18.4	18.4	18.4	18.4	18.4	8
	FCC phase	21.80	21.49	8.97	18.65	20.86	7.79
	Cu-rich phase	2.94	3.17	80.42	2.83	9.88	0
$(CoCrCuFeNi)_{88}V_{12}$	Nominal	17.6	17.6	17.6	17.6	17.6	12
	FCC phase	21.34	17.31	9.09	14.71	22.25	15.30
	Cu-rich phase	3.79	3.08	81.81	2.94	6.79	1.06
	Sigma phase	7.53	15.24	16.09	5.91	5.58	49.65
$(CoCrCuFeNi)_{84}V_{16}$	Nominal	16.8	16.8	16.8	16.8	16.8	16
	FCC phase	21.71	20.89	8.46	16.15	20.38	12.42
	Cu-rich phase	8.16	9.69	62.26	6.00	8.44	5.02
	Sigma phase	2.56	8.79	36.66	1.84	3.09	55.86

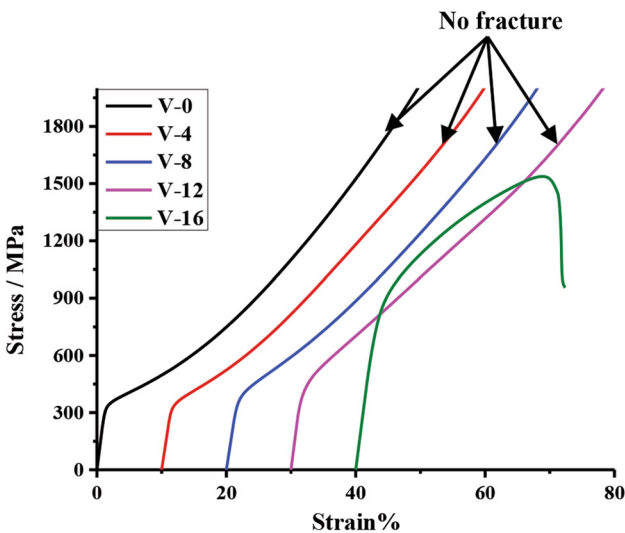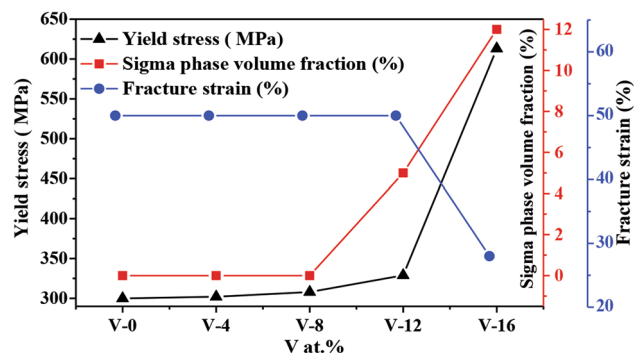**Fig. 5** Compressive engineering stress–strain curves of $(CoCrCuFeNi)_{100-x}V_x$ (x = 0-16) HEAs

Fig. 6 Effect of the volume fraction of the sigma phase (attained by Grid Statistic Method) on the yield stress and the fracture strain of $(CoCrCuFeNi)_{100-x}V_x$ HEAs

shown in Fig. 3(a), it showed that the matrix possessed a typical dendritic structure, and Cu was found precipitated as second phase in the interdendritic region. The Cu-rich phase changed to the spherical morphology from strip shape when V
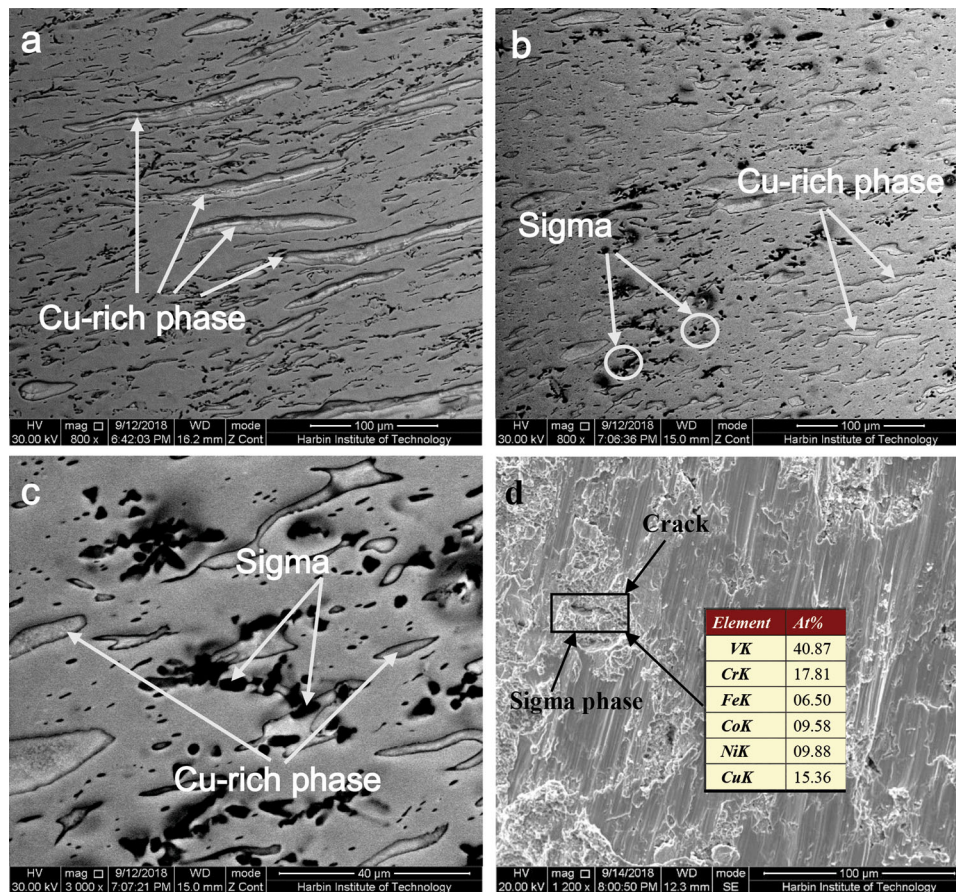
Fig. 7 Microstructural features of the deformation HEAs. (a) The microstructural features of the deformation $(CoCrCuFeNi)_{92}V_8$ HEA (backscatter signal), (b) the microstructural features of the deformation $(CoCrCuFeNi)_{88}V_{12}$ HEA (backscatter signal), (c) the high-magnification microstructural features of the deformation $(CoCrCuFeNi)_{88}V_{12}$ HEA (backscatter signal), (d) compression fracture features of the deformation $(CoCrCuFeNi)_{84}V_{16}$ HEA (secondary electron signal)
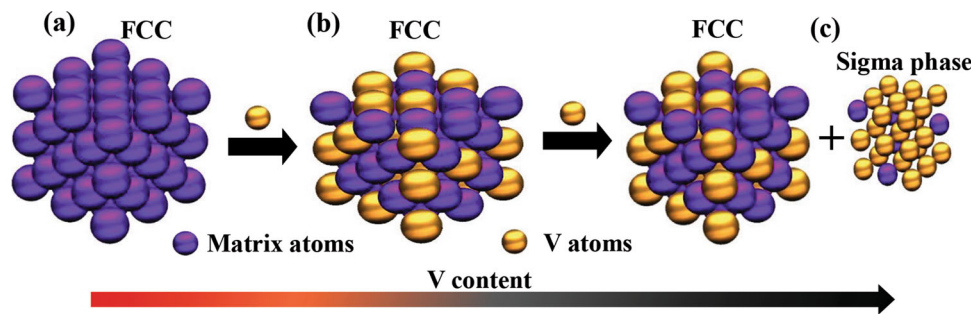

Fig. 8 Atomic diffusion model for sigma phase formation in $(CoCrCuFeNi)_{100-x}V_x$ HEAs

content increased from 4 to 8% as shown in Fig. 3(b) and (c). When V content reached 12%, the sigma phase was found in $(CoCrCuFeNi)_{88}V_{12}$ HEA (see Fig. 3d). However, the sigma phase was not tested by XRD for its thin volume fraction. The volume fraction of sigma phase increased with V content increase as shown in Fig. 3(e). Figure 3(f) shows the image of $(CoCrCuFeNi)_{84}V_{16}$ HEA with high magnification; it shows the sigma and Cu-rich phases clearly.

Figure 4 shows the elements distribution images of $(CoCrCuFeNi)_{84}V_{16}$ HEA by EDS. Table 2 shows the compositions (at.%) of various phases in as-cast $(CoCrCuFeNi)_{100-x}V_x$ (x = 0, 4, 8, 12 and 16) HEAs by EDS. They

showed that sigma phase was V-rich region and the spheroidal particles were present Cu-rich region, which indicated that V was added in CoCrCuFeNi HEA, which had positive effect in sigma phase precipitation.

Figure 5 shows the engineering stress–strain curve of $(CoCrCuFeNi)_{100-x}V_x$ HEAs measured by compressive text. As shown in Fig. 5, the yield stress of the alloy gradually increased from 300 to 613 MPa with V content increasing from 0 to 16%, while the compression fracture strain decreased from 50 to 28%. When V content was 0, 4, 8 and 12%, respectively, the compressive specimens had no fracture when the strain reached 50%.
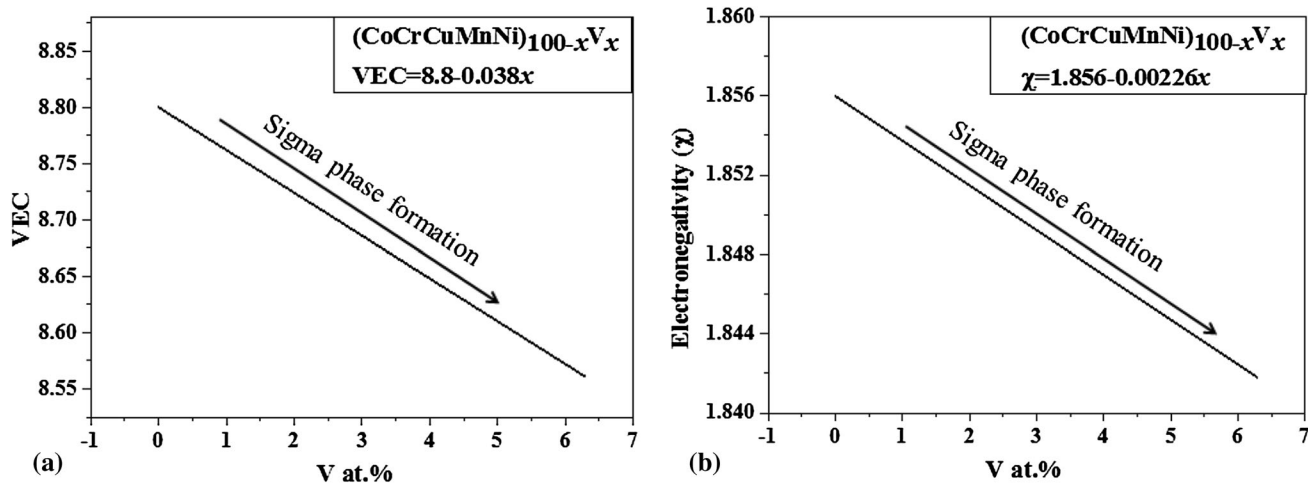
Fig. 9 (a) VEC of $(CoCrCuFeNi)_{100-x}V_x$ HEAs. (b) χ of $(CoCrCuFeNi)_{100-x}V_x$ HEAs

Figure 6 shows the effect of sigma phase volume fraction (attained by Grid Statistic Method) on the yield stress and the fracture strain of $(CoCrCuFeNi)_{100-x}V_x$ HEAs. It showed that the volume fraction of sigma phase increased gradually from 0 to 12% as the V content increased, the yield stress increased from 300 to 613 MPa, and the compression fracture strain decreased from 50 to 28%. It implied that V addition had positive effect on promoting sigma phase precipitation and improving the strength of CoCrCuFeNi HEA. According to the formula: $\delta = \delta_{fcc}V_{fcc} + \delta_{sigma}V_{sigma}$ (Ref [42]), the plasticity and strength of HEAs could be roughly estimated, where the δ_{fcc} and δ_{sigma} represent the strength of the FCC phase and sigma phase, respectively, and the V_{fcc} and V_{sigma} represent the volume fraction of the two phases, respectively. The volume fraction of the sigma phase (attained by Grid Statistic Method) gradually increased with V content increase in $(CoCrCuFeNi)_{100-x}V_x$ HEAs system. Therefore, V addition was beneficial in improving the strength of CoCrCuFeNi HEA.

In order to reveal the effects of sigma phase on the deformation and fracture process, the microstructural features of the deformation and the fracture-compressed samples were observed by SEM. Figure 7(a), (b) and (c) shows the microstructural features of the deformation $(CoCrCuFeNi)_{92}V_8$ and $(CoCrCuFeNi)_{88}V_{12}$ HEAs, and Fig. 7(d) shows the compression fracture features of the $(CoCrCuFeNi)_{84}V_{16}$ HEA. As shown in Fig. 7(a), in the process of compression deformation, the Cu-rich phases were pressed and deformed. However, the sigma phases were not deformed (see Fig. 7b and c). It was indicated that the sigma phases play a key role in improving the strength of this CoCrCuFeNi HEA. As shown in Fig. 7(d), it showed the compression fracture features of the $(CoCrCuFeNi)_{84}V_{16}$ HEA. The EDS result (Fig. 7d) showed the crack occurs on the V-rich phase (sigma phase). In the process of compression deformation, the Cu-rich phases and matrix phase were deformed; however, the sigma phases do not have enough deformability, breakdown and formation of the cracks. These cracks as a starting point lead to the fracture of the compression specimen.

For describing the process of sigma phase precipitation more clearly, an atomic diffusion model was established. As shown in Fig. 8, when V content was 0% in $(CoCrCuFeNi)_{100-x}V_x$ HEAs, the matrix of the HEA formed FCC phase structure, as shown in Fig. 8(a). When V content was low, V

atoms could be dissolved in the matrix, as shown in Fig. 8(b), which caused a large lattice distortion and improved the effect of solid-solution strength. As the V element further increased, more and more atoms were dissolved in the matrix and replaced the matrix atoms. When V content exceeded the limits of it could be dissolved in the matrix, a part of V atoms would be separated out from FCC matrix and formed sigma phase with some matrix atoms as shown in Fig. 8(c).

Valence electron concentration (VEC) and electronegativity (χ) were important physical parameters for phase formation in HEA field based on these papers (Ref [6, 41-50]). Figure 9 shows the VEC and electronegativity (χ) of $(CoCrCuFeNi)_{100-x}V_x$ HEAs. VEC could be attained by this formula: $VEC = \sum_{n=1}^{n} c_i(VEC)_i$, where the VEC of the ith component element is presented by $(VEC)_i$ and the atomic percentage of the ith component element is represented by c_i (Ref [5, 38, 45-47]). As shown in Fig. 9(a), the VEC of $(CoCrCuFeNi)_{100-x}V_x$ HEAs decreased with increasing V content. The electronegativity (χ) could be calculated by this formula: $\chi = \sum_{n=1}^{n} c_i(\chi)_i$, where χ of the ith component element is represented by $(\chi)_i$ and the atomic percentage of the ith component element is represented by c_i (Ref [6, 39]). As shown in Fig. 9(b), the value of electronegativity (χ) also decreased with increasing V content. The results indicated that the decreases in VEC and electronegativity (χ) played a positive role in promoting sigma phase formation.

4. Conclusions

The microstructure and mechanical properties of $(CoCrCuFeNi)_{100-x}V_x$ HEAs had been studied in this paper. Based on the experiment and subsequent analysis results, several conclusions could be attained as follows:

1. V addition played a positive role in sigma phase precipitation. The volume fraction of sigma phase increased from 0 to 12% with increasing V content from 0% to 16 at.%.
2. The compressive yield stress of $(CoCrCuFeNi)_{100-x}V_x$ HEAs increased from 300 to 613 MPa with V content increasing from 0 to 16%; the compression fracture strain decreased from 50 to 28%.

3. The increases in the sigma phase volume fraction played a key role in increasing the yield stress of $(CoCrCuFeNi)_{100-x}V_x$ HEAs.

References

1. J.W. Yeh, S.K. Chen, S.J. Lin, J.Y. Gan, T.S. Chin, T.T. Shun, C.H. Tsau, and S.Y. Chang, Nanostructured High-Entropy Alloys with Multiple Principal Elements: Novel Alloy Design Concepts and Outcomes, *Adv. Eng. Mater.*, 2004, **6**, p 299–303

2. B. Cantor, I.T.H. Chang, P. Knight, and A.J.B. Vincent, Microstructural Development in Equiatomic Multicomponent Alloys, *Mater. Sci. Eng. A*, 2004, **375–377**, p 213–218

3. S.J. Sun, Y.Z. Tian, H.R. Lin, X.G. Dong, Y.H. Wang, Z.J. Zhang, and Z.F. Zhang, Enhanced Strength and Ductility of Bulk CoCrFeMnNi High Entropy Alloy Having Fully Recrystallized Ultrafine-Grained Structure, *Mater. Des.*, 2017, **133**, p 122–127

4. Y. Liu, Y. Zhang, H. Zhang, N. Wang, X. Chen, H. Zhang, and Y. Li, Microstructure and Mechanical Properties of Refractory $HfMo_{0.5}Nb\text{-}TiV_{0.5}Si_x$ High-Entropy Composites, *J. Alloys Compd.*, 2017, **694**, p 869–876

5. X.W. Liu, L. Liu, G. Liu, X.X. Wu, D.H. Lu, J.Q. Yao, W.M. Jiang, Z.T. Fan, and W.B. Zhang, The Role of Carbon in Grain Refinement of Cast CrFeCoNi High-Entropy Alloys, *Metall. Mater. Trans. A*, 2018, **49**, p 2151–2160

6. Y. Zhang, T.T. Zuo, Z. Tang, Z. Tang, M. Gao, K. Dahmen, P. Liaw, and Z. Lu, Microstructures and Properties of High-Entropy Alloys, *Prog. Mater. Sci.*, 2014, **61**, p 1–93

7. Y. Zhang, Y. Liu, Y. Li, X. Chen, and H. Zhang, Microstructure and Mechanical Properties of a Refractory $HfNbTiVSi_{0.5}$ High-Entropy Alloy Composite, *Mater. Lett.*, 2016, **174**, p 82–85

8. S.J. Sun, Y.Z. Tian, H.R. Lin, H.J. Yang, X.G. Dong, Y.H. Wang, and Z.F. Zhang, Transition of Twinning Behavior in CoCrFeMnNi High Entropy Alloy with Grain Refinement, *Mater. Sci. Eng. A*, 2018, **712**, p 603–607

9. L. Yuan, C. Min, Y. Li, and X. Chen, Microstructure and Mechanical Performance of AlxCoCrCuFeNi High-Entropy Alloys, *Rare Metal Mater. Eng.*, 2009, **38**, p 1602–1607

10. Y. Lu, Y. Dong, S. Guo, L. Jiang, H.J. Kang, T.M. Wang, B. Wen, Z.J. Wang, J.C. Jie, Z.Q. Cao, H.H. Ruan, and T.J. Li, A Promising New Class of High-Temperature Alloys: Eutectic High-Entropy Alloys, *Sci. Rep.*, 2014, **4**, p 6200

11. Y. Lu, X. Gao, L. Jiang, Z. Chen, T. Wang, J. Jie, H. Kang, Y. Zhang, S. Guo, H. Ruan, Y. Zhao, Z. Cao, and T. Li, Directly Cast Bulk Eutectic and Near-Eutectic High Entropy Alloys with Balanced Strength and Ductility in a Wide Temperature Range, *Acta Mater.*, 2017, **124**, p 143–150

12. X. Gao, Y. Lu, B. Zhang, N. Liang, G. Wu, G. Sha, J. Liu, and Y. Zhao, Microstructural Origins of High Strength and High Ductility in an $AlCoCrFeNi_{2.1}$ Eutectic High-Entropy Alloy, *Acta Mater.*, 2007, **141**, p 59–66

13. B. Wang, A. Fu, X. Huang, B. Liu, Y. Liu, Z. Li, and X. Zan, Mechanical Properties and Microstructure of the CoCrFeMnNi High Entropy Alloy Under High Strain Rate Compression, *J. Mater. Eng. Perform.*, 2016, **25**, p 2985–2992

14. C. Zhang, G.F. Wu, and P.Q. Dai, Phase Transformation and Aging Behavior of $Al_{0.5}CoCrFeNiSi_{0.2}$, *High-Entropy Alloy. J. Mater. Eng. Perform.*, 2015, **24**, p 1918–1925

15. J.Q. Yao, X.W. Liu, N. Gao, Q.H. Jiang, N. Li, G. Liu, W.B. Zhang, and Z.T. Fan, Phase Stability of a Ductile Single-Phase BCC $Hf_{0.5}Nb_{0.5}Ta_{0.5}Ti_{1.5}Zr$ Refractory High-Entropy Alloy, *Intermetallics*, 2018, **98**, p 79–88

16. R. Chen, G. Qin, H. Zheng, L. Wang, S. Yanqing, Y. Chiu, H. Ding, J. Guo, and F. Hengzhi, Composition Design of High Entropy Alloys Using the Valence Electron Concentration to Balance Strength and Ductility, *Acta Mater.*, 2018, **144**, p 129–137

17. G. Qin, W. Xue, C. Fan, R. Chen, L. Wang, S. Yanqing, H. Ding, and J. Guo, Effect of Co Content on Phase Formation and Mechanical Properties of $(AlCoCrFeNi)_{100-x}Co_x$ High-Entropy Alloys, *Mater. Sci. Eng. A*, 2018, **710**, p 200–205

18. G. Qin, S. Wang, R. Chen, X. Gong, L. Wang, Y. Su, J. Guo, and H. Fu, Microstructures and Mechanical Properties of Nb-Alloyed CoCrCuFeNi High-Entropy Alloys, *J. Mater. Sci. Technol.*, 2018, **34**, p 365–369

19. X. Jin, Y. Zhou, L. Zhang, and X.B. Li, A New Pseudo Binary Strategy to Design Eutectic High Entropy Alloys Using Mixing Enthalpy and Valence Electron Concentration, *Mater. Des.*, 2018, **143**, p 49–55

20. L. Zhang, Y. Zhou, X. Jin, X. Du, and B. Li, The Microstructure and High-Temperature Properties of Novel Nano Precipitation-Hardened Face Centered Cubic High-Entropy Superalloys, *Scr. Mater.*, 2018, **146**, p 226–230

21. Y. Dong, L. Jiang, Z. Tang, Y. Lu, and T. Li, Effect of Electromagnetic Field on Microstructure and Properties of Bulk $AlCrFeNiMo_{0.2}$, *High-Entropy Alloy. J. Mater. Eng. Perform.*, 2015, **24**, p 4475–4481

22. L. Tian, Z.M. Jiao, G.Z. Yuan, S.G. Ma, Z.H. Wang, H.J. Yang, Y. Zhang, and J.W. Qiao, Effect of Strain Rate on Deformation Behavior of AlCoCrFeNi High-Entropy Alloy by Nanoindentation, *J. Mater. Eng. Perform.*, 2016, **25**, p 2255–2260

23. A. Li, D. Ma, and Q. Zheng, Effect of Cr on Microstructure and Properties of a Series of $AlTiCr_x$ FeCoNiCu High-Entropy Alloys, *J. Mater. Eng. Perform.*, 2014, **23**, p 1197–1203

24. N.D. Stepanov, D.G. Shaysultanov, G.A. Salishchev, M.A. Tikhonovsky, E.E. Oleynik, A.S. Tortika, and O.N. Senkov, Effect of V Content on Microstructure and Mechanical Properties Of the $CoCrFeMnNiV_x$, High Entropy Alloys, *J. Alloys Compd.*, 2015, **628**, p 170–185

25. X.F. Wang, Y. Zhang, Y. Qiao, and G.L. Chen, Novel Microstructure and Properties of Multicomponent $CoCrCuFeNiTi_x$ Alloys, *Intermetallics*, 2007, **15**, p 357–362

26. J.Y. He, W.H. Liu, H. Wang, Y. Wu, X.J. Liu, T.G. Nieh, and Z.P. Lu, Effects of Al Addition on Structural Evolution and Tensile Properties of the FeCoNiCrMn High-Entropy Alloy System, *Acta Mater.*, 2014, **62**, p 105–113

27. B.S. Li, Y.P. Wang, M.X. Ren, C. Yang, and H.Z. Fu, Effects of Mn, Ti and V on the Microstructure and Properties of AlCrFeCoNiCu High Entropy Alloy, *Mater. Sci. Eng. A*, 2008, **498**(1–2), p 482–486

28. Y. Dong, K. Zhou, Y. Lu, X. Gao, T.M. Wang, and T. Li, Effect of Vanadium Addition on the Microstructure and Properties of AlCoCrFeNi High Entropy Alloy, *Mater. Des.*, 2014, **57**, p 67–72

29. W.R. Wang, W.L. Wang, S.C. Wang, Y.C. Tsai, C.-H. Lai, and J.W. Yeh, Effects of Al Addition on the Microstructure and Mechanical Property of $Al_xCoCrFeNi$ High-Entropy Alloys, *Intermetallics*, 2012, **26**(7), p 44–51

30. W.H. Liu, Z.P. Lu, J.Y. He, J.H. Luan, Z.J. Wang, B. Liu, Y. Liu, and M.W. Chen, Ductile $CoCrFeNiMo_x$ High Entropy Alloys Strengthened By Hard Intermetallic Phases, *Acta Mater.*, 2016, **116**, p 332–342

31. F. He, Z. Wang, P. Cheng, Q. Wang, J.J. Li, Y.Y. Dang, J.C. Wang, and C.T. Liu, Designing Eutectic High Entropy Alloys of $CoCrFeNiNb_x$, *J. Alloys Compd.*, 2015, **656**, p 284–289

32. S.G. Ma and Y. Zhang, Effect of Nb Addition on the Microstructure And Properties of AlCoCrFeNi High-Entropy Alloy, *Mater. Sci. Eng. A*, 2012, **532**, p 480–486

33. Y. Zhang, Y.J. Zhou, J.P. Lin, G.L. Chen, and P.K. Liaw, Solid-Solution Phase Formation Rules for Multi-Component Alloys, *Adv. Eng. Mater.*, 2008, **10**, p 534–538

34. W.H. Liu, J.Y. He, H.L. Huang, H. Wang, Z.P. Lu, and C.T. Liu, Effects of Nb Additions on the Microstructure and Mechanical Property of CoCrFeNi High-Entropy Alloys, *Intermetallics*, 2015, **60**, p 1–8

35. J. Chen, P. Niu, Y. Liu, and J. Liu, Effect of Zr Content on Microstructure and Mechanical Properties of AlCoCrFeNi High Entropy Alloy, *Mater. Des.*, 2016, **94**, p 39–44

36. T. Egami and Y. Waseda, Atomic Size Effect on the Formability of Metallic Glasses, *J. Non-Cryst. Solids*, 1984, **64**, p 113–134

37. W. Jackson, Characterization of BCC Phases in $AlCoCrFeNiTi_x$ High Entropy Alloys, *Mater. Lett.*, 2015, **138**, p 78–80

38. J.M. Zhu, H.M. Fu, H.F. Zhang, A.M. Wang, H. Li, and Z.Q. Hu, Synthesis and Properties of Multiprincipal Component AlCoCrFeNi-Si_x, *Alloys. Mater. Sci. Eng. A*, 2010, **527**, p 7210–7214

39. X. Yang and Y. Zhang, Prediction of High-Entropy Stabilized Solid-Solution in Multi-Component Alloys, *Mater. Chem. Phys.*, 2012, **132**, p 233–238

40. Z. Li, K.G. Pradeep, and Y. Deng, Metastable High-Entropy Dual-Phase Alloys Overcome the Strength-Ductility Trade-off, *Nature*, 2016, **534**, p 227–230

41. Y. Zhang, Z.P. Lu, S.G. Ma, P.K. Liaw, Z. Tang, Y.Q. Cheng, and M.C. Gao, Guidelines in Predicting Phase Formation of High-Entropy Alloys, *Mrs Commun.*, 2014, **42**, p 57–62

42. S.W. Tsai, *Theory of Composites Design*, Think Composites Press, 1992

43. S. Guo, C. Ng, J. Lu, and C.T. Liu, Effect of Valence Electron Concentration on Stability of FCC or BCC Phase in High Entropy Alloys, *J. Appl. Phys.*, 2011, **109**, p 645–647

44. S. Guo and C.T. Liu, Phase Stability in High Entropy Alloys: Formation of Solid-Solution Phase or Amorphous Phase, *Prog. Nat. Sci. : Mater. Int.*, 2011, **21**, p 433–446

45. S. Fang, X. Xiao, X. Lei, W. Li, and Y. Dong, Relationship Between the Widths of Supercooled Liquid Regions and Bond Parameters of Mg-Based Bulk Metallic Glasses, *J. Non-Cryst. Solids*, 2003, **321**(1), p 120–125

46. M.H. Tsai, K.Y. Tsai, C.W. Tsai, C. Lee, C.C. Juan, and J.W. Ye, Criterion for Sigma Phase Formation in Cr- and V-Containing High-Entropy Alloys, *Mater. Res. Lett.*, 2013, **1**, p 207–212

47. M.H. Tsai, K.C. Chang, J.H. Li, J.H. Li, R.C. Tsai, and A.C. Hung, A Second Criterion for Sigma Phase Formation in High-Entropy Alloys, *Mater. Res. Lett.*, 2016, **4**, p 1–6

48. R. Feng, M.C. Gao, C. Lee, M. Mathes, T. Zuo, S. Chen, J.A. Hawk, Y. Zhang, and P.K. Liaw, Design of Light-Weight High-Entropy Alloys, *Entropy*, 2016, **18**, p 333

49. M.C. Troparevsky, J.R. Morris, P.R.C. Kent, A.R. Lupini, and G.M. Stocks, Criteria for Predicting the Formation of Single-Phase High-Entropy Alloys, *Phys. Rev. X*, 2015, **5**, p 1–6

50. N. Yurchenko, N. Stepanov, and G. Salishchev, Laves-Phase Formation Criterion for High-Entropy Alloys, *Met. Sci. J.*, 2016, **33**, p 17–22